

## Molecular Orbital Calculations on Dinitrogen-Bridged Transition-Metal Dimers

CYNTHIA B. POWELL and MICHAEL B. HALL\*

Received February 28, 1984

Fenske-Hall molecular orbital calculations on  $[\{\text{Ru}(\text{NH}_3)_5\}_2(\text{N}_2)]^{4+}$ ,  $[\{\text{Nb}(\text{PH}_3)_2(\text{CH}_2)(\text{CH}_3)_2\}_2(\text{N}_2)]$ ,  $[\{\text{Zr}(\text{C}_5\text{H}_5)_2(\text{N}_2)\}_2(\text{N}_2)]$ , and  $[\{\text{Re}(\text{PH}_3)_4\text{Cl}\}\{\text{MoCl}_4(\text{OH})\}_2(\text{N}_2)]$  are reported. These molecules model  $\mu\text{-N}_2$  dimers in which the N-N bond lengths vary from 1.124 to 1.298 Å. The calculated Mulliken populations of the  $\mu\text{-N}_2$   $1\pi_g$  orbitals decrease in the order Nb dimer > Zr dimer > Re-Mo dimer > Ru dimer, which is also the order of decreasing bond length as determined by X-ray crystallography. Our calculations suggest that more electrons are donated into the  $\mu\text{-N}_2$   $1\pi_g$  system in the Nb, Zr, and Re-Mo cases because of the presence of unoccupied  $d\pi$  orbitals, which are at higher energy than occupied  $d\pi$  orbitals and stabilize the  $\mu\text{-N}_2$   $1\pi_g$  MO. These orbitals also allow delocalization of the  $\mu\text{-N}_2$   $1\pi_g$  electrons, which alleviates charge buildup. Differences between the Nb and Zr dimer M-N and N-N bond strengths are enhanced by synergetic  $\sigma$  donation in the Nb dimer.

## Introduction

Research in the area of nitrogen fixation has heightened interest in the nature of transition metal-dinitrogen interactions. Dinitrogen exhibits a variety of bonding modes. Several dimeric species contain nearly linear bridging  $\text{N}_2$  units. Comparisons between these complexes reveal relatively large differences in N-N bond lengths.<sup>1</sup>

Table I lists N-N bond lengths for free dinitrogen, dimethyldiazine, hydrazine, and representative  $\mu\text{-dinitrogen}$  transition-metal complexes.  $[\{\text{Ru}(\text{NH}_3)_5\}_2(\text{N}_2)]^{4+}$ , which was the first of the  $\mu\text{-N}_2$  complexes characterized by X-ray crystallography, has a N-N bond length of 1.124 Å.<sup>2</sup> The longest  $\mu\text{-N}_2$  bond lengths, 1.282 and 1.298 Å, are reported for two tantalum dimers synthesized by Schrock and co-workers.<sup>3a,b</sup> Several other niobium and tantalum dimers have also been prepared.<sup>3</sup> Although no crystallographic data for the niobium complexes have been reported, they are assumed to have analogous structures. Similar zirconium<sup>4</sup> and titanium<sup>5</sup> dimers have shorter N-N bond lengths of 1.182 and 1.165 Å, respectively. The unsymmetrical complex  $[\{\text{Re}(\text{PMe}_2\text{Ph})_4\text{Cl}\}\{\text{MoCl}_4(\text{OMe})\}_2(\text{N}_2)]$  also has a long bond length of 1.18 Å.<sup>6</sup>

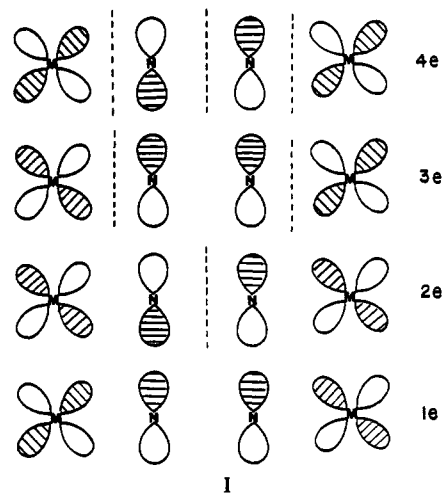
Rocklage and Schrock have called attention to the puzzling bond length differences observed for the  $[\{\text{Ta}(\text{CHCMe}_3)(\text{PMe}_3)_2(\text{CH}_2\text{CMe}_3)\}_2(\text{N}_2)]$  dimer and the zirconium and titanium dimers.<sup>3a,c,d</sup> The molecular geometries are related, and formal electron counts assign each metal center a  $d^2$  configuration. In addition, both react with anhydrous HCl to yield hydrazine.<sup>7</sup> The tantalum complex will also produce di-

Table I

complex	$d(\text{M-N})$ , Å	$d(\text{N-N})$ , Å	ref
$\text{N}_2$		1.0976	9
$\text{N}_2\text{Me}_2$		1.23	10
$\text{N}_2\text{H}_4$		1.46	10
$[\{\text{Ti}(\eta^5\text{-C}_5\text{Me}_5)_2\}_2(\text{N}_2)]$	2.010 (10)	1.165 (4)	5
$[\{\text{Zr}(\eta^5\text{-C}_5\text{Me}_5)_2(\text{N}_2)\}_2(\text{N}_2)]$	2.081	1.182 (5)	4
$[\{\text{Ta}(\text{CHCMe}_3)(\text{PMe}_3)_2(\text{CH}_2\text{CMe}_3)\}_2(\text{N}_2)]$	1.8395	1.298	3a
$[\{\text{TaCl}_3(\text{P}(\text{bz})_3)(\text{THF})\}_2(\text{N}_2)]$	1.796 (5)	1.282 (6)	3b
$[\{\text{Mo}(\eta^5\text{-C}_5\text{H}_5\text{Me}_3)(\text{CO})_2\}_2(\text{N}_2)]$	2.042 (4)	1.145 (7)	12
$[\{\text{Mn}(\eta^5\text{-C}_5\text{H}_4\text{Me})(\text{CO})_2\}_2(\text{N}_2)]$	1.875 (5)	1.118 (7)	1b
$[\{\text{Re}(\text{PMe}_3\text{Ph})_4\text{Cl}\}\{\text{MoCl}_4(\text{OMe})\}_2(\text{N}_2)]$	1.815 (15)	1.18 (3)	6
	1.90 (1)		
	(Mo)		
$[\{\text{Fe}(\text{CO})_2(\text{P}(\text{OMe})_3)\}_2(\text{N}_2)]$	1.876 (9)	1.13 (1)	11
$[\{\text{Ru}(\text{NH}_3)_5\}_2(\text{N}_2)]^{4+}$	1.928	1.124 (15)	2
$[\{\text{Ni}(\text{PCy}_3)_2\}_2(\text{N}_2)]$	1.78	1.12	13

methylketazine when combined with acetone.<sup>3</sup> Such reactions are consistent with a formal description of the bridging dinitrogen as an  $\text{N}_2^{4-}$  ligand.

The simple qualitative molecular orbital scheme pictured in **1** has been used to describe the four-center M-N-N-M



interactions.<sup>1</sup> It has been suggested that the longer N-N distances observed for dimers with fewer than 10 d electrons are a result of the fact that an orbital like the 3e MO in **1** is not filled. However, this diagram does not offer an explanation for the relatively large differences in N-N bond length observed for complexes containing similar metal ions and an equal number of d electrons.

Electronic structures of isolated  $\mu\text{-N}_2$  complexes have been calculated, but the result have been used primarily to predict

- (a) Chatt, J.; Dilworth, J. R.; Richards, R. L. *Chem. Rev.* **1978**, *78*, 589. (b) Chatt, J., Ed. "New Trends in the Chemistry of Nitrogen Fixation"; Academic Press: London, 1978. (c) Sellman, D. *Angew. Chem.* **1974**, *86*, 692.
- (a) Treitel, I. M.; Flood, M. T.; Marsh, R. E.; Gray, H. B. *J. Am. Chem. Soc.* **1969**, *91*, 6512. (b) Fergusson, J. E.; Love, J. L.; Robinson, W. T. *Inorg. Chem.* **1972**, *11*, 1662.
- (a) Turner, H. W.; Fellman, J. D.; Rocklage, S. M.; Schrock, R. R.; Churchill, M. R.; Wasserman, H. J. *J. Am. Chem. Soc.* **1980**, *102*, 7811. (b) Churchill, M. R.; Wasserman, H. J. *Inorg. Chem.* **1982**, *21*, 218. (c) Rocklage, S. M.; Turner, H. W.; Fellman, J. D.; Schrock, R. R. *Organometallics* **1982**, *1*, 703. (d) Rocklage, S. M.; Schrock, R. R. *J. Am. Chem. Soc.* **1982**, *104*, 3077.
- (a) Sanner, R. D.; Manriquez, J. M.; Marsh, R. E.; Bercaw, J. E. *J. Am. Chem. Soc.* **1976**, *98*, 8351.
- (a) Sanner, R. D.; Duggan, D. M.; McKenzie, T. C.; Bercaw, J. E. *J. Am. Chem. Soc.* **1976**, *98*, 8358.
- (a) Mercer, M.; Crabtree, R. H.; Richards, R. L. *Chem. Soc., Chem. Commun.* **1973**, 808. (b) Mercer, M. *J. Chem. Soc., Dalton* **1974**, 1637.
- (a) Bercaw, J. E.; Rozenburg, E.; Roberts, J. D. *J. Am. Chem. Soc.* **1974**, *96*, 612. However, Bercaw and co-workers have done an extensive labeling study of the reaction between  $\mu\text{-N}_2$  zirconium dimers and HCl. Their results suggest that the terminal  $\text{N}_2$  ligands are involved in hydrazine formation. This is supported by the fact that dimers in which terminal  $\text{N}_2$  ligands are replaced by CO do not react to produce hydrazine. (b) Manriquez, J. M.; Sanner, R. D.; Marsh, R. E.; Bercaw, J. E. *J. Am. Chem. Soc.* **1976**, *98*, 3042.

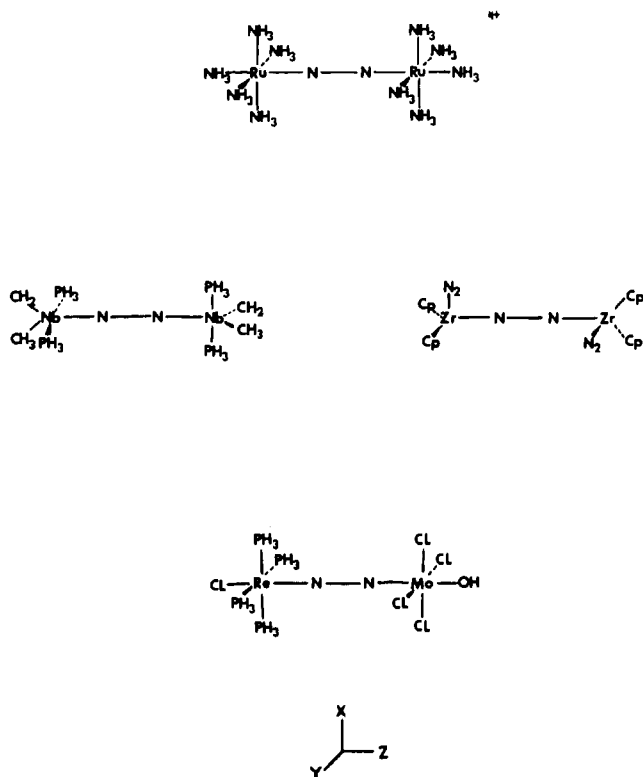


**Figure 1.** Molecular geometries of  $[\{\text{Ru}(\text{NH}_3)_5\}_2(\text{N}_2)]^{4+}$ ,  $[\{\text{Nb}(\text{C}_5\text{H}_5)(\text{CH}_3)(\text{PH}_3)_2\}_2(\text{N}_2)]$ ,  $[\{\text{ZrCp}_2(\text{N}_2)_2\}_2(\text{N}_2)]$ , and  $[\{\text{Re}(\text{PH}_3)_4\text{Cl}\}[\text{MoCl}_4(\text{OH})]]_2(\text{N}_2)$  that were used in the calculations. Our coordinate system is also shown.

preferred molecular conformations.<sup>8</sup> In their discussion of the conformations of bridged dimers, Kostić and Fenske briefly examined the M–N bonding in  $\mu\text{-N}_2$  dimers.<sup>8a</sup> A comprehensive review of quantum-mechanical contributions to the study of nitrogen fixation was recently published,<sup>9</sup> and Rappé has reported ab initio calculations on  $[\text{Cl}_4\text{MoN}]_2$ .<sup>10</sup> We present here the results of a systematic study focusing on the dinitrogen–transition metal interactions, which help clarify the causes of N–N bond length variation. Fenske–Hall calculations were performed on four  $\mu\text{-N}_2$  dimers. The model complexes  $[\{\text{Zr}(\text{C}_5\text{H}_5)_2(\text{N}_2)_2\}_2(\text{N}_2)]$ ,  $[\{\text{Nb}(\text{PH}_3)_2(\text{CH}_2)(\text{CH}_3)\}_2(\text{N}_2)]$ ,  $[\{\text{Re}(\text{PH}_3)_4\text{Cl}\}[\text{MoCl}_4(\text{OH})]]_2(\text{N}_2)$ , and  $[\{\text{Ru}(\text{NH}_3)_5\}_2(\text{N}_2)]^{4+}$  were studied. They were chosen as representative of extremes in bond length. As previously mentioned, comparisons between the electronic structures of the zirconium and niobium complexes are of special interest. The N–N bond length in the ruthenium dimer is one of the shortest observed, and the novel rhenium–molybdenum complex provides a second example of a N–N bond intermediate in length that involves very different metal systems.

### Experimental and Theoretical Calculations

Fenske–Hall molecular orbital calculations<sup>16</sup> were performed on a VAX 11/780 computer at Texas A&M University. The zirconium, niobium, molybdenum, and ruthenium basis functions were taken from

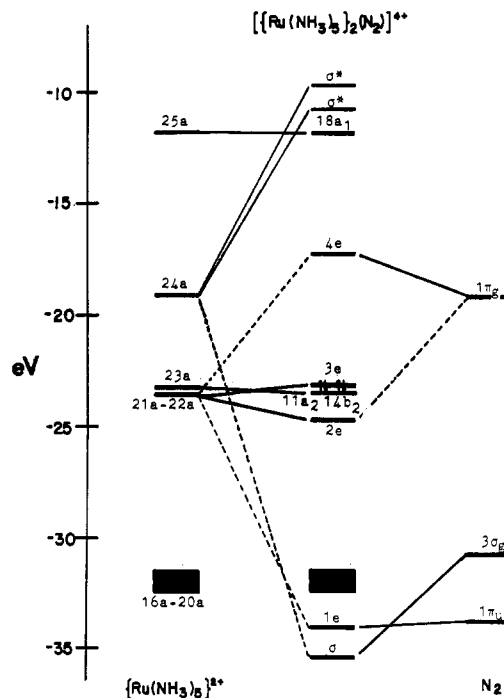


**Figure 2.** Molecular orbital diagram calculated for the  $[\{\text{Ru}(\text{NH}_3)_5\}_2(\text{N}_2)]^{4+}$  dimer.

Richardson<sup>17,18</sup> and were augmented by 5s and 5p functions with exponents of 2.20.<sup>19</sup> Since suitable third-row transition-metal functions are not available, technetium functions were used in place of rhenium. The carbon, oxygen, nitrogen, phosphorus, and chlorine functions were taken from the double- $\zeta$  basis set of Clementi.<sup>20</sup> The core and valence s functions were reduced to single- $\zeta$  functions. An exponent of 1.2 was used for hydrogen atoms. Mulliken population analysis was used to determine both the individual atomic charges and atomic orbital populations. Overlap populations between atoms were calculated and used to predict trends in bond strength. The program MOPLOT<sup>21</sup> was used to plot the wave functions of molecular orbitals.

Molecular geometries (Figure 1) were idealized from crystal structures of similar complexes. The crystal structure of  $[\{\text{Zr}(\text{C}_5\text{Me}_5)_2(\text{N}_2)_2\}_2(\text{N}_2)]$  was used as a basis for setting the bond distances and angles for the Zr dimer,<sup>4</sup> the mixed-metal dimer was patterned after  $[\{\text{Re}(\text{PMe}_2\text{Ph})_4\text{Cl}\}[\text{MoCl}_4(\text{OMe})]]_2(\text{N}_2)$ ,<sup>6</sup> and the geometry of the Nb complex was taken from crystal data for  $[\{\text{Ta}(\text{CHCMe}_3)(\text{PMe}_3)_2(\text{CH}_2\text{CMe}_3)_2\}_2(\text{N}_2)]$ .<sup>3a</sup> The crystal structure of  $[\{\text{Ru}(\text{NH}_3)_5\}_2(\text{N}_2)]^{4+}$  has been published.<sup>2</sup> The Zr and Nb complexes were idealized to  $C_2$  symmetry, and the ligand bond angles of the Re–Mo dimer were adjusted to  $90^\circ$ , as were the Ru–NH<sub>3</sub> bond angles. All M–N distances were set at 1.96 Å, and the N–N bond distance for the bridging N<sub>2</sub> units were set at 1.24 Å, so that overlaps could be validly compared. These values are the averages of the bond lengths in the Zr–N–N–Zr and Ta–N–N–Ta systems.

Figure 1 shows our right-handed coordinate system. The results are described in terms of these coordinates; the  $d_{z^2}$  orbitals of each metal atom point toward the N atoms, the  $d_{xz}$  and  $d_{yz}$  orbitals are  $\pi$ -type orbitals, and the  $d_{xy}$  and  $d_{x^2-y^2}$  are  $\delta$ -type orbitals. For the N atoms, the  $p_z$  orbitals form a  $\sigma$  N–N bond and the  $p_x$  and  $p_y$  orbitals form the N  $\pi$  bonds.

In large molecules, the complexity of the MO pattern causes difficulties in interpretation. An alternative to analyzing molecular orbitals in terms of atomic orbital composition is analysis on the basis of preformed fragments. This approach can simplify interpretation

- (8) (a) Kostić, N. M.; Fenske, R. F. *J. Organomet. Chem.* **1982**, *233*, 337.  
(b) Hoffmann, R.; Thorn, D. L.; Shilov, A. E. *Koord. Khim.* **1977**, *3*, 1260.
- (9) Pelikán, P.; Boča, R. *Coord. Chem. Rev.* **1984**, *55*, 55.
- (10) Rappé, A. K. *Inorg. Chem.* **1984**, *23*, 995.
- (11) Wilkinson, P. G.; Houk, N. B. *J. Chem. Phys.* **1956**, *24*, 528.
- (12) "Interatomic Distances"; The Chemical Society: London, 1958.
- (13) Berke, H.; Bankhardt, W.; Huttner, G.; Seyer, J.; Zsolnai, L. *Chem. Ber.* **1981**, *114*, 2754.
- (14) Ziegler, M. L.; Weidenhammer, K.; Zeinn, H.; Skell, R.; Herrmann, W. A. *Angew. Chem., Int. Ed. Engl.* **1976**, *15*, 695.
- (15) Jolly, P. W.; Jonas, K.; Krüger, C.; Tsay, U.-H. *J. Organomet. Chem.* **1971**, *33*, 1971.
- (16) Hall, M. B.; Fenske, R. F. *Inorg. Chem.* **1972**, *11*, 768.

- (17) Richardson, J. W.; Nieuwpoort, W. C.; Powell, R. R.; Edgell, W. F. *J. Chem. Phys.* **1962**, *36*, 1057.
- (18) Richardson, J. W.; Blackman, M. J.; Ranochak, J. E. *J. Chem. Phys.* **1973**, *58*, 3010.
- (19) Barber, M.; Connor, J. A.; Guest, M. F.; Hall, M. B.; Hillier, I. H.; Meredith, W. N. E. *J. Chem. Soc., Faraday Trans. 2* **1972**, *54*, 219.
- (20) "Tables of Atomic Functions", a supplement to a paper by: Clementi, E. *IBM J. Res. Dev.* **1965**, *9*, 2.
- (21) Lichtenberger, D. L. Ph.D. Dissertation, University of Wisconsin, Madison, WI, 1974.

Table II. Mulliken Populations of  $\mu$ -N<sub>2</sub> MOs in Dimers

complex	2 $\sigma_g$	2 $\sigma_u$	1 $\pi_u$	3 $\sigma_g$	1 $\pi_g$
{[Nb(CH <sub>2</sub> )(CH <sub>3</sub> )(PH <sub>3</sub> ) <sub>2</sub> ] <sub>2</sub> (N <sub>2</sub> )}	2.041	1.658	1.965	1.429	0.757
{[ZrCp <sub>2</sub> (N <sub>2</sub> )] <sub>2</sub> (N <sub>2</sub> )}	2.044	1.655	1.963	1.452	0.725
{[Re(PH <sub>3</sub> ) <sub>4</sub> Cl][MoCl <sub>4</sub> (OH)](N <sub>2</sub> )}	2.033	1.687	1.970	1.450	0.584
{[Ru(NH <sub>3</sub> ) <sub>5</sub> ] <sub>2</sub> (N <sub>2</sub> ) <sup>4+</sup> }	2.032	1.704	2.007	1.449	0.432

Table III. Mulliken Populations of Upper Metal Fragment MOs

{Ru(NH <sub>3</sub> ) <sub>5</sub> } <sup>2+</sup>		{Nb(CH <sub>2</sub> )(CH <sub>3</sub> )(PH <sub>3</sub> ) <sub>2</sub> }		{ZrCp <sub>2</sub> (N <sub>2</sub> )}		populn	
MO	populn	MO	populn	MO	populn	MO	{Re(PH <sub>3</sub> ) <sub>4</sub> Cl} {MoCl <sub>4</sub> (OH)}
21a	1.780	17a	1.068	32a	1.208	21a	1.990 2.000
22a	1.780	18a	0.371	33a	0.410	22a	1.203 1.006
23a	1.990	19a	0.026	34a	0.006	23a	1.476 0.360
24a	0.405	20a	0.227	35a	0.002	24a	0.436 0.000
25a	0.000	21a	0.072	36a	0.124	25a	0.020 0.463

and has been used successfully to describe bonding in cluster systems.<sup>22</sup> In the calculations reported in this paper each molecule was divided into three fragments: the bridging N<sub>2</sub> unit and each metal atom with its terminal ligands.

### Results and Discussion

{[Ru(NH<sub>3</sub>)<sub>5</sub>]<sub>2</sub>(N<sub>2</sub>)<sup>4+</sup>}. The electronic structure of the upper valence region of {[Ru(NH<sub>3</sub>)<sub>5</sub>]<sub>2</sub>(N<sub>2</sub>)<sup>4+</sup>} is shown in Figure 2. The diagram depicts MOs for two {Ru(NH<sub>3</sub>)<sub>5</sub>}<sup>2+</sup> metal fragments interacting with MOs of a bridging N<sub>2</sub> unit to produce the energy levels shown in the center of the diagram. Each Ru metal is coordinated by five NH<sub>3</sub> ligands in octahedral sites. The sixth site is vacant in the metal fragment but occupied by the N<sub>2</sub> ligand in the full molecule. The dimer has C<sub>2v</sub> symmetry due to the arrangement of the hydrogen atoms.

Metal fragment MOs 21a, 22a, and 24a are involved in Ru–N–N–Ru bonding. These MOs, along with the 23a and 25a levels, are primarily Ru 4d in character. They have been split by interactions with the terminal NH<sub>3</sub> ligands. MO 23a is the HOMO for the independent fragment and is doubly occupied. The block-labeled 16a–20a represent closely spaced MOs that are Ru–NH<sub>3</sub>  $\sigma$  bonding orbitals and are nonbonding with respect to the bridging N<sub>2</sub> unit.

On the right side of Figure 2, the 3 $\sigma_g$ , 1 $\pi_u$ , and 1 $\pi_g$  MOs of the diatomic N<sub>2</sub> unit are depicted. The 3 $\sigma_g$  and 1 $\pi_u$  levels are both bonding in character and are fully occupied so that the diatomic fragment before interactions with the metal fragments has a formal triple bond. The 1 $\pi_g$  orbital is unoccupied, but close in energy to occupied MOs on the ruthenium fragment.

As a matter of convenience, the MOs of the full molecule that have  $\sigma$  and  $\sigma^*$  N–metal character or are generated by interactions of the N<sub>2</sub> 1 $\pi_u$  or 1 $\pi_g$  MOs with metal fragment MOs have been labeled  $\sigma$  or  $\sigma^*$  and 1e, 2e, 3e, or 4e, respectively. These labels will be used throughout our discussion of the other calculations. Orbitals that are nonbonding with respect to the M–N–N–M bridging system are labeled according to the appropriate molecular symmetry, which is C<sub>2v</sub> in this case.

The lowest energy MO shown on the diagram for {[Ru(NH<sub>3</sub>)<sub>5</sub>]<sub>2</sub>(N<sub>2</sub>)<sup>4+</sup>} is the  $\sigma$  bonding orbital formed by the stabilization of the N<sub>2</sub> 3 $\sigma_g$  orbital through interactions with the unoccupied 24a Ru fragment MO. Tables II and III list the Mulliken populations of important fragment MOs as calculated for the full molecules. The N<sub>2</sub> 3 $\sigma_g$  predictably shows a decrease in population, while the previously unoccupied 24a orbitals have populations of 0.40 electrons. The 2 $\sigma_u$  orbital, which is not shown on the MO diagram, is stabilized by approximately 1.6 eV. It also interacts with MO 24a and shows a decrease in population.

The MO labeled 1e is only weakly bonding between the Ru atoms and the N<sub>2</sub> bridge. Its character is almost purely N<sub>2</sub> 1 $\pi_u$ , although it is slightly stabilized by Ru fragment MOs 21a and 22a, which correspond to the d<sub>xz</sub> and d<sub>yz</sub> orbitals. The simple qualitative scheme shown in 1 implies that an orbital exists that is nearly equal in metal and nitrogen character and is bonding between each of the four centers. Our calculations suggest that the N<sub>2</sub> 1 $\pi_u$  orbitals do not interact strongly enough with the Ru orbitals to contribute much to metal–N<sub>2</sub> bonding.<sup>23</sup> Mulliken populations remain virtually unchanged for the 1 $\pi_u$  levels in the independent Ru fragment and in the dimer; no electron density is transferred from the 1 $\pi_u$  orbitals to the Ru centers.

Interactions between Ru fragment MOs 21a and 22a and the N<sub>2</sub> 1 $\pi_g$  orbital form the MO labeled 2e. This orbital corresponds quite closely to the 2e MO in 1. Although the metal orbitals are closer in energy to the final MO, strong interactions with the 1 $\pi_g$  orbital allow nearly equivalent Ru and N<sub>2</sub> character. Previously unoccupied 1 $\pi_g$  levels have Mulliken populations of 0.43, while MOs 21a and 22a have lost electrons and show populations of 1.78 in the dimer.

The 3e MO for {[Ru(NH<sub>3</sub>)<sub>5</sub>]<sub>2</sub>(N<sub>2</sub>)<sup>4+</sup>}, like the 1e MO, is almost nonbonding with respect to M–N–N–M interactions. It is only slightly destabilized by interaction with the N<sub>2</sub> 1 $\pi_u$  MO. Again, these results differ from the simple qualitative scheme presented in 1. Whereas the 3e MO in 1 has an equal mixture of metal and N<sub>2</sub> character, the Ru dimer 3e MO is almost entirely Ru 4d in character. The 3e MO is the HOMO of the molecule. Another nonbonding orbital comprised of Ru 4d character is located just below the 3e level in energy.

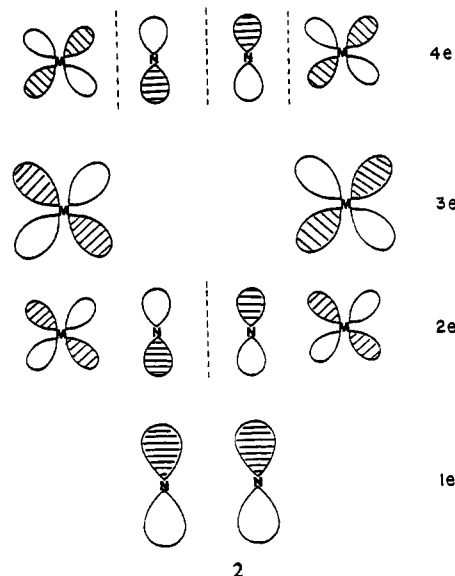
MO 4e is antibonding between all four centers and corresponds well with the 4e orbital depicted in 1. It is the LUMO of {[Ru(NH<sub>3</sub>)<sub>5</sub>]<sub>2</sub>(N<sub>2</sub>)<sup>4+</sup>}. Unoccupied MO 18a<sub>1</sub> is a nonbonding MO, and the MOs labeled  $\sigma^*$  are antibonding combinations of the Ru fragment 24a and N<sub>2</sub> 3 $\sigma_g$  orbitals.

A more accurate general scheme for the Ru–N–N–Ru bonding MOs is pictured in 2. Nonbonding  $\delta$ -type orbitals are not included. Since the levels would be filled through the 3e MO in 1 and 2, they predict equivalent Ru–N bond orders and N–N bond orders.

{[Nb(PH<sub>3</sub>)<sub>2</sub>(CH<sub>2</sub>)(CH<sub>3</sub>)<sub>2</sub>](N<sub>2</sub>)}. Figure 3 shows the electronic structure of the upper valence region of {[Nb(PH<sub>3</sub>)<sub>2</sub>(CH<sub>2</sub>)(CH<sub>3</sub>)<sub>2</sub>](N<sub>2</sub>)}. The MOs for {Nb(PH<sub>3</sub>)<sub>2</sub>(CH<sub>2</sub>)(CH<sub>3</sub>)<sub>2</sub>} fragments are shown interacting with MOs of a bridging N<sub>2</sub> unit to produce the diagram for the full molecule. The ligands in the {Nb(PH<sub>3</sub>)<sub>2</sub>(CH<sub>2</sub>)(CH<sub>3</sub>)<sub>2</sub>} fragment are arranged around the metal atom in a distorted trigonal-bipyramidal fashion. PH<sub>3</sub> ligands occupy axial sites, and the alkyl and alkylidene

(22) (a) Schilling, B. E.; Hoffmann, R. J. *Am. Chem. Soc.* **1979**, *101*, 3456. (b) Chesky, P. T.; Hall, M. B. *Inorg. Chem.* **1981**, *20*, 4419.

(23) Kostić and Fenske (see ref 8a) mention similar M–N–N–M interactions when reporting results of calculations in which they were examining the preferred molecular conformations.



2

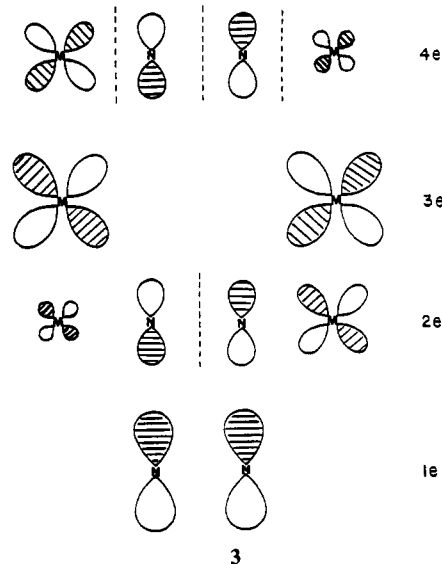
ligands occupy two of the three equatorial sites, the third being vacant.

The Nb fragment orbitals 9a, 10a, and 11a are C-H bonding orbitals for the CH<sub>3</sub> and CH<sub>2</sub> ligands. They do not have significant Nb character. MO 12a is a Nb d-P  $\sigma$ -bonding combination. MO 14a also has P lone pair character but is more weakly bonding. The C p<sub>z</sub> orbital of the CH<sub>2</sub> ligand interacts with Nb d orbitals to form MO 13a, which is  $\sigma$  bonding, while MO 16a is CH<sub>2</sub> C-Nb  $\pi$  bonding in character. MO 15a is the CH<sub>3</sub> C-Nb  $\sigma$  bonding orbital. These interactions destabilize and split the Nb d orbitals to a greater degree than in the Ru dimer. Only the doubly occupied HOMO, which is MO 17a, remains at the same energy. MOs 17a-20a are primarily Nb 4d in character. The Nb 5s orbital contributes some character to MO 18a, while MO 20a has some Nb 5p character, and MO 21a is mostly Nb 5p. MO 19a is the CH<sub>2</sub> Nb-C  $\pi^*$  orbital.

The HOMO of the dimer is labeled 2e and is fully occupied. Fragment MOs 17a, 18a, 19a, 20a, 21a, 22a, 23a, and 24a are nonbonding with respect to the N<sub>2</sub> bridge, and their characters have already been discussed. They are shown as blocks on the MO diagram. The orbital labeled  $\sigma$  is a bonding combination of the Nb 18a and 21a MOs with the N<sub>2</sub> 3 $\sigma_g$  orbital. Also contributing to  $\sigma$  bonding, but not shown on the diagram, is the N<sub>2</sub> 2 $\sigma_u$  orbital, which interacts with MO 18a and is stabilized by 1.75 eV. The Mulliken populations show that both of the N<sub>2</sub> orbitals (the 2 $\sigma_u$  and 3 $\sigma_g$ ) decrease in electron population, while 0.37 electron is gained in the metal fragment 18a MO and 0.07 electron is gained in the 21a MO.

As in the Ru case, the 1e MO for the Nb dimer is only slightly stabilized by interactions with d orbitals. This MO can be considered primarily N<sub>2</sub>  $\pi$  bonding in nature; it does not contribute significantly to M-N bonding, although a small amount of N<sub>2</sub>  $\pi \rightarrow$  metal donation is observed in Mulliken populations. In contrast to the MO scheme for the Ru dimer, the 2e and 3e MOs both contain N<sub>2</sub> 1 $\pi_g$  character. The d<sub>xz</sub> and d<sub>yz</sub> orbitals are split by terminal ligand interactions. As a result the interactions with the N<sub>2</sub> 1 $\pi_g$  orbital are altered. They are most easily understood as the combination of *in-phase* and *out-of-phase* d<sub>xz</sub> and d<sub>yz</sub> orbitals with the  $\pi^*$  network.

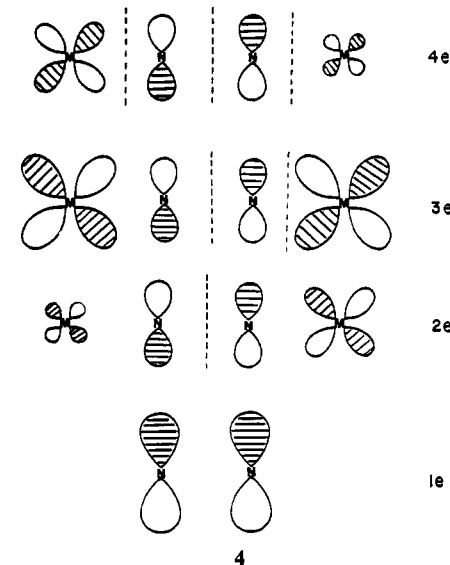
3 represents the orbitals that would be expected to result from the interactions of d<sub>xz</sub> and d<sub>yz</sub> orbitals that are separated by a sizable energy gap with the N<sub>2</sub>  $\pi^*$  network. The smaller participation by one metal d orbital in the 2e and 4e MOs occurs because of the geometry of the Nb dimer. Although each half of the molecule is identical, one side is rotated 90° with respect to the other. This causes the d<sub>xz</sub> orbital of one



3

metal atom to be equivalent to the d<sub>yz</sub> orbital of the other, and vice versa. On the MO diagram in Figure 3, MOs 17a and 20a participate in forming both the 2e and 3e orbitals.

In 3, as in the Ru case, N<sub>2</sub> 1 $\pi_u$  orbitals are shown not to interact with the *in-phase* d orbitals. The MOs actually observed, however, show mixing of the N<sub>2</sub> 1 $\pi_g$  orbitals with the nonbonding 3e MO as shown in 4. If the fragment MO had



4

pure d-orbital character, an interaction would not be allowed. Mixing occurs by an indirect mechanism because of the near degeneracy of the 3e nonbonding d orbital combination and the N<sub>2</sub> 1 $\pi_g$  level. Thus, the 2e orbital of [Nb(PH<sub>3</sub>)<sub>2</sub>(C-H<sub>2</sub>)(CH<sub>3</sub>)<sub>2</sub>(N<sub>2</sub>)] corresponds reasonably well to the 2e MO pictured in 1. The 3e MO, on the other hand, does not. It is antibonding in character between the nitrogen atoms and between Nb and N, while bonding between the second Nb and N. Still, it has overall nonbonding character since the degenerate orbitals are mirror images of each other. Contour plots are quite helpful in describing these MOs and will be presented in a following section. It is important to note, however, that the N<sub>2</sub> 1 $\pi_g$  population is much greater in the Nb dimer than in the Ru dimer and that the 17a MOs, which are the HOMOs in the Nb fragments, have donated 0.93 electron while the 20a MOs, which were previously vacant, are now occupied by 0.37 electron. The 4e MO is located at ~4 eV and corresponds to the 4e MO in 1 quite closely.

[{Zr(C<sub>5</sub>H<sub>5</sub>)<sub>2</sub>(N<sub>2</sub>)<sub>2</sub>(N<sub>2</sub>)}. The electronic structure of the upper valence region of [Zr(C<sub>5</sub>H<sub>5</sub>)<sub>2</sub>(N<sub>2</sub>)<sub>2</sub>(N<sub>2</sub>)] is shown in

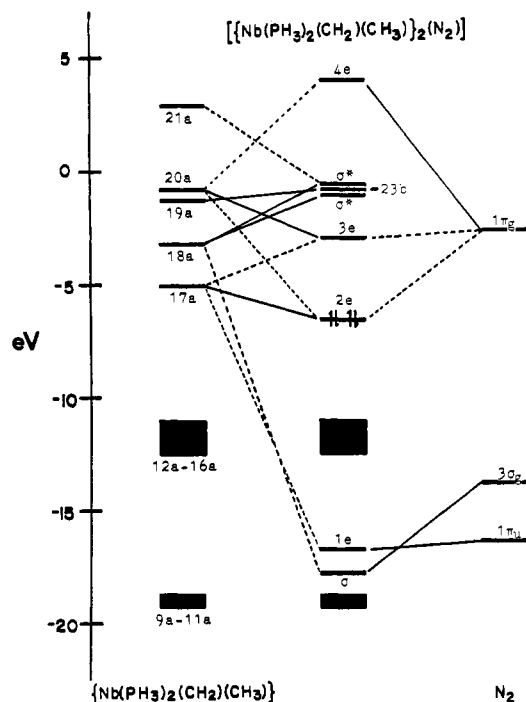


Figure 3. Molecular orbital diagram for the  $[\{\text{Nb}(\text{CH}_2)(\text{CH}_3)(\text{P}-\text{H}_3)_2\}_2(\text{N}_2)]$  dimer.

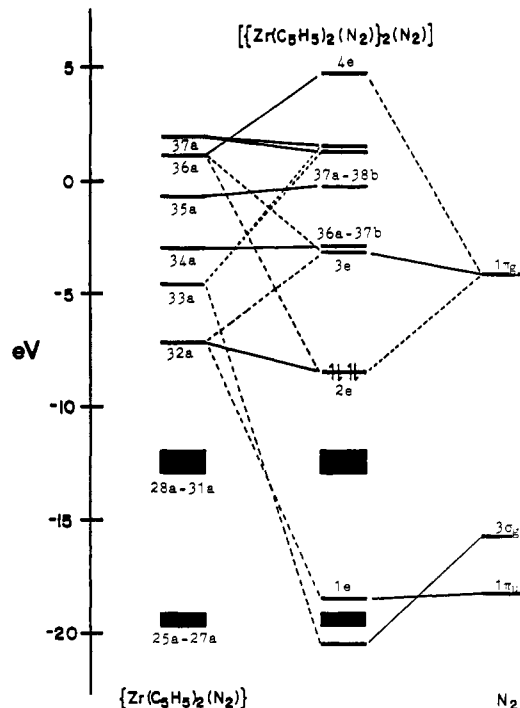


Figure 4. Molecular orbital diagram for the  $[\{\text{ZrCp}_2(\text{N}_2)\}_2(\text{N}_2)]$  dimer.

Figure 4. This diagram depicts MOs for two  $\{\text{Zr}(\text{C}_5\text{H}_5)_2(\text{N}_2)\}$  fragments interacting with MOs for a bridging  $\text{N}_2$  unit to form the energy levels shown in the center. The metal fragments are composed of two  $\eta^5$ -cyclopentadienyl rings and a linearly bound  $\text{N}_2$  ligand coordinating a Zr atom. The ligands occupy tetrahedral type sites, although distorted from tetrahedral angles.

MO 25a is formed by the interaction of the terminal  $\text{N}_2$   $3\sigma_g$  orbitals with the Zr  $d_{z^2}$  orbital. MOs 26a and 27a are localized on the Cp rings and do not contribute to metal-Cp bonding. MOs 28a-31a are Cp  $1e''$  in character and are stabilized by the Zr d orbitals. The unique feature of the Zr fragment MO pattern is the stabilization of MO 32a, the HOMO, due to interactions with the terminal  $\text{N}_2$   $1\pi_g$  orbital. As a result, this level is lower in energy than the corresponding Nb fragment MO, although the neutral atom Zr d orbitals would be higher in energy than neutral Nb d orbitals. The other Zr d orbitals are destabilized by the ligand interactions mentioned previously. MOs 33a, 36a, and 37a are primarily metal d in character. The Zr 5s orbital contributes some character to MO 33a, and MO 37a has some Zr 5p character. The terminal  $\text{N}_2$   $1\pi_g$  orbitals are split by their interactions with the Zr AOs and form Zr fragment MOs 34a and 35a.

Although the stabilization of the Zr fragment HOMO is the major difference between the Nb and Zr MO schemes, the other metal d orbitals are also split and destabilized to different extents. Thus, the Zr  $d_{z^2}$  orbital, and unoccupied  $\pi$ -type orbitals, are each destabilized to a greater extent than the corresponding Nb MOs. Also, the MO that corresponds to the  $d_{xy}$  orbital for the Nb fragment is much lower in energy than the  $d_{xy}$  MO of the Zr fragment.

For the full molecule, MO 2e is the HOMO and is fully occupied. Solid blocks represent MOs nearly equivalent to metal fragment MOs 25a, 26a, 27a, 28a, 29a, 30a, and 31a, which have already been described in terms of character. These orbitals are nonbonding with respect to the M-N-N-M framework. The lowest lying MO shown on the diagram is the  $\sigma$ -bonding combination of the  $\text{N}_2$   $2\sigma_u$  MO, which is stabilized  $\sim 2$  eV by interactions with MO 33a. Nearly equivalent amounts are donated from the  $\text{N}_2$   $2\sigma_u$  MOs in both the

Nb and Zr cases, but significantly more electrons are donated by the  $\mu$ - $\text{N}_2$   $3\sigma_g$  MO to the Nb atom even though the  $\mu$ - $\text{N}_2$   $3\sigma_g$  MO in the Zr dimer is stabilized to a greater extent. Although this seems unusual, it can be explained in terms of simple two orbital interactions. Equation 1 describes the

$$\epsilon \propto H_{ij}^2 / (H_{ii} - H_{jj}) \quad (1)$$

dependence of stabilization energy on orbital interaction ( $H_{ij}$ ) and orbital energy separation ( $H_{ii} - H_{jj}$ ). Calculations using this formula show that the greater Zr-N<sub>2</sub> interaction offsets the larger  $H_{ii} - H_{jj}$  term, causing greater stabilization, while the Nb level's closer proximity allows more electron donation. It should also be noted that in the Nb case, unlike the Zr case, a second metal orbital, fragment MO 21a, accepts electrons from the  $\text{N}_2$   $3\sigma_g$  orbital.

In terms of orbital character, the Zr dimer 2e and 3e MOs are very similar to the Nb MOs, with the exception of the terminal  $\text{N}_2$   $1\pi_g$  character seen in the Zr dimer orbitals. Mulliken populations show fewer electrons in the bridging  $\text{N}_2$   $1\pi_g$  MO for the Zr dimer than for the Nb dimer. This is consistent with the larger population in the Zr fragment MO 32a than in the Nb 17a MO and the smaller electron population for the Zr 36a MO than for the Nb 20a MO. The larger  $\mu$ - $\text{N}_2$   $1\pi_g$  population implies a longer N-N bond for the Nb dimer.

Metal fragment MOs 34a and 35a are terminal  $\text{N}_2$  in character and nonbonding with respect to the  $\mu$ - $\text{N}_2$  ligand. The levels labeled  $\sigma^*$  have M-N  $\sigma^*$  character originating from MO 33a and  $\text{N}_2$   $3\sigma_g$  interactions but also contain large contributions from the Zr fragment MO 37a, which is nonbonding in character. MO 4e is antibonding between all four atoms in the M-N-N-M bridge and corresponds to the 4e MO in 1 quite well.

$[\{\text{Re}(\text{PH}_3)_4\text{Cl}\}\{\text{MoCl}_4(\text{OH})\}(\text{N}_2)]$ . The electronic structure of  $[\{\text{Re}(\text{PH}_3)_4\text{Cl}\}\{\text{MoCl}_4(\text{OH})\}(\text{N}_2)]$  is shown in Figure 5. There are 48 doubly occupied MOs, and the HOMO is singly occupied. The latter orbital is one of the nearly degenerate 3e orbitals. Again, the large blocks are Re fragment MOs 14a-20a and Mo fragment MOs 6a-20a, which are nonbonding with respect to M-N-N-M interactions. These MOs include metal to terminal ligand bonding orbitals as well as

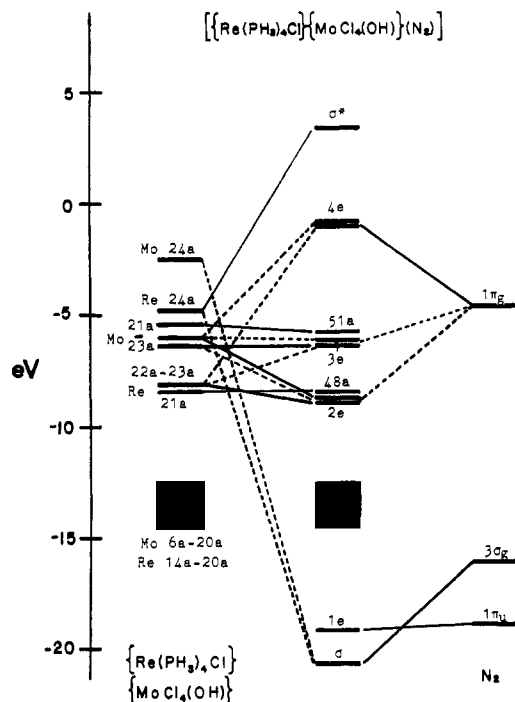


**Figure 5.** Molecular orbital diagram for the  $[\{\text{Re}(\text{PH}_3)_4\text{Cl}\}]\{\text{MoCl}_4(\text{OH})\}(\text{N}_2)$  dimer.

lower lying orbitals localized on the terminal ligands. Re fragment MO 21a and Mo fragment MO 34a are also M–N–N–M nonbonding orbitals. The MO diagram, in general, is much more complex than the previous examples discussed, since the halves of the molecule are not identical. We will not spend a lot of time detailing each interaction but will concentrate on those factors that may contribute to N–N bond lengthening.

The  $\sigma$  bonding orbital formed by the interaction of the Mo fragment 24a MO and the Re fragment 24a MO with the  $\text{N}_2$   $3\sigma_g$  orbital is the lowest energy level shown on the diagram. As in the previous cases, the  $\text{N}_2$   $2\sigma_u$  orbital also interacts with both 24a MOs and is stabilized by  $\sim 1.7$  eV. Although the  $2\sigma_u$  donation is slightly less than that observed for either the Nb or Zr dimer, the  $3\sigma_g$  orbital donation is nearly equivalent to that observed for the Zr dimer. The 1e orbital, like each of the others, is almost entirely  $\text{N}_2$   $\pi$  bonding in character. Only a small amount of  $1\pi_u$  to metal donation is indicated by Mulliken populations.

Nearly degenerate orbitals are labeled "2e" and "3e" and parallel the Nb and Zr dimer MOs. Mo fragment MOs 21a and 22a and Re fragment MOs 22a and 23a are primarily  $d_{xz}$  and  $d_{yz}$  in character. The *in-phase* and *out-of-phase* combinations of these orbitals with the  $\text{N}_2$   $1\pi_g$  orbitals form the 2e and 3e sets. The Mo fragment MOs have been pushed up in energy by  $\pi$ -donor ligands and consequently are closer to the  $\text{N}_2$   $1\pi_g$  orbitals. Although the Mo orbitals are stabilized to a greater extent, Mulliken populations show no net donation into the  $1\pi_g$  system. This might be expected since Mo fragment 21a is the HOMO of the independent fragment and is only occupied by 1 electron. The 22a MO of the Mo unit accepts electrons and has a population of 0.36 in the full molecule. Re fragment MOs 22a and 23a are both doubly occupied in the independent fragment; the 23a MO is the HOMO. Donation out of each of these orbitals into the  $\text{N}_2$   $1\pi_g$  orbital is observed. The  $\text{N}_2$   $1\pi_g$  population is 0.58 electron, which is intermediate between the Zr and Nb dimer and the Ru dimer  $1\pi_g$  populations.

The 4e MO is antibonding between all four of the bridge atoms, as in each previous case. Re fragment 24a orbital

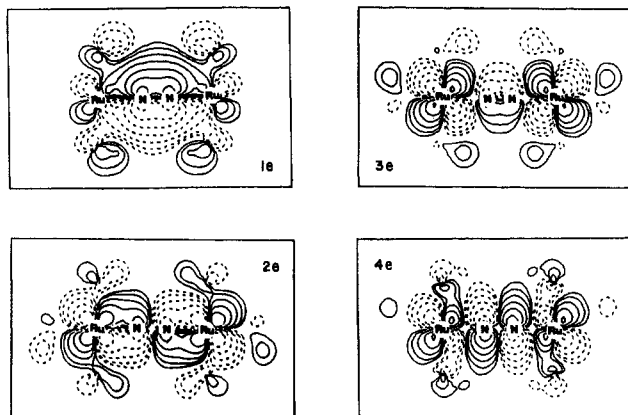


**Figure 6.** Molecular orbital plots of the 1e, 2e, 3e, and 4e MOs for  $[\{\text{Ru}(\text{NH}_3)_5\}_2(\text{N}_2)]^{4+}$  in the  $xz$  plane.

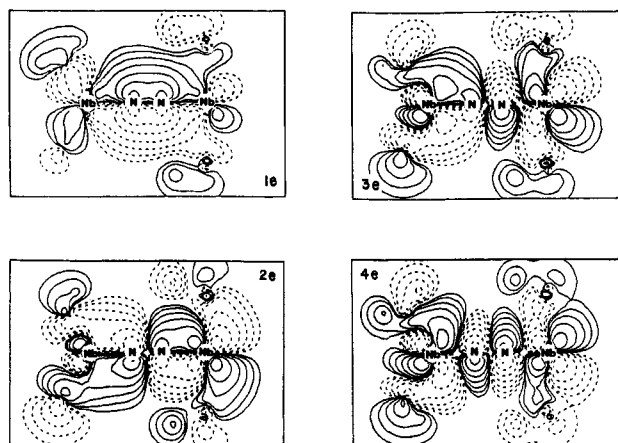


**Figure 7.** Molecular orbital plots of the 1e, 2e, 3e, and 4e MOs for  $[\text{Nb}(\text{CH}_2(\text{CH}_3)(\text{PH}_3)_2)_2(\text{N}_2)]$  in the  $xz$  plane.

interactions with the  $\text{N}_2$   $3\sigma_g$  orbital form the MO labeled  $\sigma^*$ . The Mo fragment– $\text{N}_2$   $\sigma^*$  orbital is located higher in energy and is not shown on this diagram.

**Molecular Orbital Plots.** In order to clarify the differences in the bonding of  $\mu$ - $\text{N}_2$  dimers better, the MOs important to M–N–N–M  $\pi$ -type interactions were plotted. Plots can be helpful since individual bonds may be delocalized over several MOs. The 1e, 2e, 3e, and 4e MOs are shown for each dimer. All of the maps are plotted in the  $yz$  planes. In each case only one of the two degenerate orbitals is pictured; the others have their maxima in the  $xz$  planes and are mirror images of the  $yz$  plots, with the exception of the mixed-metal dimer. For  $[\{\text{Re}(\text{PH}_3)_4\text{Cl}\}]\{\text{MoCl}_4(\text{OH})\}(\text{N}_2)$  each orbital in the near degenerate sets have equivalent Re fragment,  $\text{N}_2$ , and Mo fragment contours.

Figure 6 shows MO plots for the Ru  $\mu$ - $\text{N}_2$  dimer. As in all of the plots shown, each contour is a factor of 2 different from its neighbor. The outside contour marked is  $3.91 \times 10^{-3} \text{ e/au}^2$ . This is  $1/256 \text{ e/au}^3$  or  $0.026 \text{ e/\AA}^3$ . The solid lines are positive contours, and the dashed lines are negative contours. Thus, it is evident that the  $[\{\text{Ru}(\text{NH}_3)_5\}_2(\text{N}_2)]^{4+}$  1e MO is primarily bridging  $\text{N}_2$  in character, since each N atom is surrounded by three more contours than the Ru atoms. Likewise, the 3e orbital shows some  $\text{N}_2$   $1\pi_u$  character, but the d orbitals have two more contours, indicating that the  $\mu$ - $\text{N}_2$  contributions to this MO are small. The plots show that MOs 2e and 4e have nearly equivalent  $\text{N}_2$   $1\pi_g$  and Ru  $d_{yz}$  character, as has already been noted.

The 1e, 2e, 3e, and 4e MOs of the Nb dimer are shown in Figure 7. Again, the greatly dominant  $\text{N}_2$   $1\pi_u$  character of the 1e MO is evident. A conspicuous difference between the plot of the Ru dimer 2e MO and the Nb dimer 2e MO is the

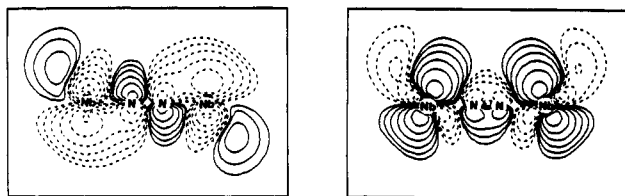
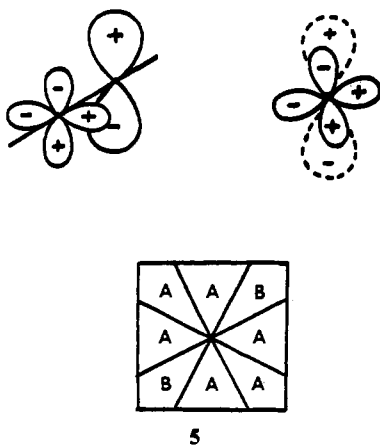


Figure 8. Molecular orbital plots of the 3e MO for  $[\{\text{Nb}(\text{CH}_2)(\text{C}-\text{H}_3)(\text{PH}_3)_2\}_2(\text{N}_2)]$  in the plane containing the  $C_2$  axis and the plane perpendicular to the  $C_2$  axis.

absence of symmetry in M–N–N–M interactions. As expected from previous discussion, one metal  $d_{yz}$  orbital contributes much more to the character of the MO than the second  $d_{yz}$  orbital. The pictured orbital is essentially bonding between one Nb and N, antibonding between the two N atoms, and nonbonding between the second Nb and N. In addition, the N atoms in the Nb 2e plots have one more contour than the N atoms in the Ru 2e MO. This supports the Mulliken population data, which indicate a higher  $\mu\text{-N}_2$   $1\pi_g$  occupation for the Nb dimer.

Nb dimer MO 3e has nearly equivalent amounts of metal d orbital and  $\text{N}_2$   $1\pi_g$  character, as is evident in the plot. The contour map also shows minor terminal ligand– $\text{N}_2$  interactions that encourage the mixing of the *in-phase* d orbitals with the  $1\pi_g$  orbital although this interaction in the “bare” M–N–N–M network is not allowed by symmetry. The two metal centers have different character in this plot, but the molecule contains a  $C_2$  axis, which makes the Nb atoms equivalent. Plots in the plane of the axis should have a center of inversion, and the plot in the perpendicular plane should contain a mirror plane. Figure 8 shows the Nb dimer 3e MO in the plane containing the  $C_2$  axis and the plane perpendicular to the  $C_2$  axis. The plane containing the  $C_2$  axis shows a small  $1\pi_u$  antibonding interaction with the d orbitals.

It is unusual to see both  $\pi$  and  $\pi^*$  character in one MO, but its presence can be explained as follows. In each orbital of the degenerate set, the N p character is nearly evenly divided between  $p_x$  and  $p_y$  on one N atom, while almost entirely  $p_x$  or  $p_y$  on the other N atom. A slight rotation of the orbitals with respect to each other allows the unusual combination of  $\text{N}_2$   $1\pi_u$  and  $1\pi_g$  character within a single MO as shown by 5. A plane cut through the region labeled A would show



5

antibonding character, but a plane cut through the region labeled B would have some bonding character. The  $C_2$  plane is in a B region.

The plot of the 4e MO of  $[\{\text{Nb}(\text{PH}_3)_2(\text{CH}_2)(\text{CH}_3)\}_2(\text{N}_2)]$  shows more Nb  $d_{yz}$  character for the metal atom that has less  $d_{yz}$  character in the 2e MO, and vice versa. It is antibonding between all four centers, though more weakly antibonding between one metal and N in each orbital of the e set due to the smaller  $d_{yz}$  contributions.

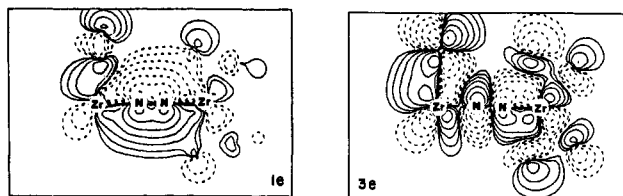


Figure 9. Molecular orbital plots of the 1e, 2e, 3e, and 4e MOs for  $[\{\text{ZrCp}_2(\text{N}_2)\}_2(\text{N}_2)]$  in the  $xz$  plane.

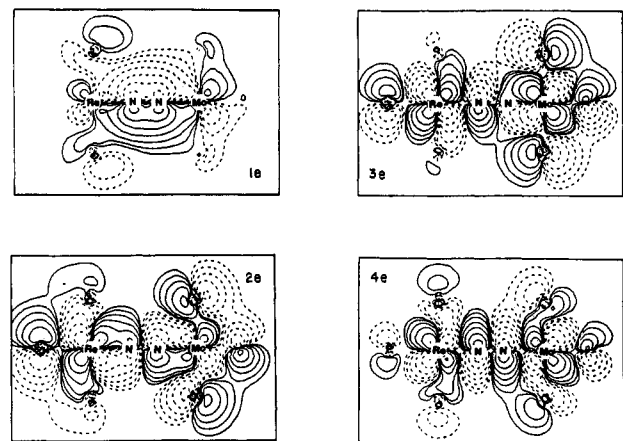


Figure 10. Molecular orbital plots of the 1e, 2e, 3e, and 4e MOs for  $[\{\text{Re}(\text{PH}_3)_4\text{Cl}\}\{\text{MoCl}_4(\text{OH})\}(\text{N}_2)]$  in the  $xz$  plane.

Plots for the Zr dimer are displayed in Figure 9. They are very similar to the contour maps for the Nb dimer. Again, the 1e MO is almost entirely  $\text{N}_2$   $1\pi_u$  in character. The 2e MO shows large terminal  $\text{N}_2$   $1\pi_g$  participation and also differs from the Nb plot in that there is even less  $d_{yz}$  character donated by one of the Zr atoms. This is not surprising since the energy gap between Zr fragment MO 32a and MO 35a is much greater than the separation between Nb fragment MOs 17a and 20a. Large terminal  $\text{N}_2$   $1\pi_g$  contours are also seen in the 3e MO. Plots of the plane containing the  $C_2$  axis and the plane perpendicular to the  $C_2$  axis are not shown but have character quite similar to those of the Nb dimer 3e orbital. An equivalent N p orbital distribution allows both  $1\pi_u$  and  $1\pi_g$  character in the 3e MO, but again the  $1\pi_u$  character is negligible. The 4e MO is antibonding between all four centers but has minimal participation by the  $d_{yz}$  orbital, which is farthest away in energy.

The last set of contour maps are the 1e, 2e, 3e, and 4e MOs of the mixed-metal dimer shown in Figure 10. These plots are unique in that they are essentially identical in both the  $yz$  and  $xz$  planes. As a result, the M–N–N–M interactions are more symmetrical. The 1e MO is nearly equivalent to the  $\text{N}_2$   $1\pi_g$  orbital. The 2e MO looks more like the plot of the Ru dimer 2e MO than the Nb or Zr dimer, although there is less Mo atom participation than Re atom participation. This is due to the fact that the Mo fragment 21a and 22a MOs have less d orbital and more terminal ligand character and are located higher in energy than the Re fragment 22a and 23a MOs. The mixed-metal dimer 2e MO also differs from the Ru dimer 2e MO in that there are fewer  $\text{N}_2$   $\pi^*$  contours in

the latter. There is equal metal d orbital and  $N_2$   $1\pi_g$  character in the 3e MO as in each previous case, even though the N atom nearest the Mo atom has half the number of contours. In this orbital, the N atom nearest the Mo atom has half the number of contours. In this orbital, the N atom nearest the Re atom is pure  $p_y$  in character, but the N atom character on the Mo end is equally divided between the  $p_x$  and  $p_y$  orbitals. Since there are two orbitals in the 3e set, the net N  $p_x$  and  $p_y$  characters are the same. The 4e MO is antibonding between each of the four bridge centers and has more  $N_2$   $1\pi_g$  character than metal  $d_{yz}$  character.

**Population Analysis.** Tables II and III show the Mulliken populations of the  $\mu$ - $N_2$  MOs and the metal fragment MOs that participate in M-N-N-M bonding. The fractional occupations reflect the electron redistribution that occurs when the metal fragments and bridging ligand interact to form the full molecules. For the  $\mu$ - $N_2$  MOs, the greatest differences between the dimers are observed in the  $1\pi_g$  orbital. On the basis of  $N_2$   $1\pi_g$  populations alone, the N-N bonds would be expected to decrease in strength in the order  $\mu$ - $N_2$  (Ru) >  $\mu$ - $N_2$  (Re-Mo) >  $\mu$ - $N_2$  (Zr) >  $\mu$ - $N_2$  (Nb). This is consistent with observed N-N bond distance differences.

It is somewhat surprising that the Nb and Zr  $N_2$   $1\pi_g$  populations are so close and that the Zr and Re-Mo dimer  $1\pi_g$  populations are not closer. This is partially due to the fact that the M-N and N-N bond distances used are the averages of the values for  $\{[Zr(C_5Me_5)_2(N_2)]_2(N_2)\}$  and  $\{[Ta(CHCMe_3)(PMe_3)_2(CH_2CMe_3)_2(N_2)]\}$ . We used these values since we were especially interested in comparisons between the Zr and Ta dimers, and the same values were used for each calculation so that overlap populations would not be weighted in favor of shorter bond distances. Since the M-N distances are actually shorter than the value used for each molecule except the Zr dimer, M-N overlaps were underestimated in the Nb, Ru, and Re-Mo cases but overestimated in the Zr case. Although the populations contain this systematic error, which was built in on purpose, they show the important trends in M-N-N-M bonding.<sup>24</sup>

Direct comparisons between the Ru dimer and mixed-metal dimer bonding interactions are rather complex. The Ru-N interaction terms are larger than the Re-N or Mo-N interaction terms, but the Re and Mo MOs are each closer to the  $N_2$   $1\pi_g$  MO in energy than the Ru MOs. These two factors balance each other to an extent. Major differences in M  $\rightarrow$   $N_2$   $1\pi_g$  donation are due to the number of d electrons and the d-orbital spacings. Ru dimer MOs 21a and 22a are degenerate and fully occupied. They each donate 0.22 electron to the  $N_2$   $\pi^*$  system. The Mo fragment orbitals 22a and 23a, on the other hand, are higher in energy than Re fragment orbitals 22a and 23a. Both of the Re fragment MOs are fully occupied, but the 23a MO of the Mo fragment is empty and the 22a MO is occupied by a single electron. The higher energy Mo fragment MOs have two effects. They stabilize the  $N_2$   $1\pi_g$  orbitals and alleviate charge buildup on the bridging ligand by allowing delocalization of the  $N_2$   $1\pi_g$  MO into the empty d orbital. These effects encourage more Re  $d\pi \rightarrow N_2$   $1\pi_g$  donation. As a result, 0.8 electron is donated from Re fragment MO 22a, which opposes the empty Mo fragment orbital, and 0.53 electron is donated from Re fragment 23a, which opposes the Mo fragment orbital containing a single electron.

On going from the mixed-metal dimer to the Zr dimer, the cylindrical symmetry of the system is destroyed. Each Zr fragment has a filled  $d\pi$  MO and an unoccupied  $d\pi$  MO at higher energy. The halves of the molecule are rotated and "locked" at 90°. This aligns the filled MO on one Zr center

with the empty MO on the other Zr center. Although the empty d orbitals are much farther in energy from the  $N_2$   $1\pi_g$  orbitals in the Zr case than they are in the Re-Mo case, they still stabilize the  $1\pi_g$  MO and encourage  $d\pi \rightarrow N_2$   $1\pi_g$  donation. Since there is one empty d orbital on each metal atom, M  $\rightarrow 1\pi_g \rightarrow$  M electron flow can occur in both directions without changing metal atom charges. This mechanism is not available to the Re-Mo dimer where the similar flow of electrons would build up charge on the Mo atom. Thus, 0.8 electron is donated from the Zr fragment 32a MOs, and the 36a MO on each Zr center accepts 0.12 electron.

Bercaw and co-workers have previously suggested  $\mu$ - $N_2$   $\pi^*$ -metal delocalization to help explain the rotated and locked structure of the Zr dimer.<sup>5</sup> In a very insightful discussion they recognize that the orbital that interacts with the  $N_2$   $1\pi_g$  MO is also of the correct symmetry to interact with the terminal  $N_2$  ligand. Our work supports this idea.

The Nb dimer M-N-N-M bonding framework is very similar to that for the Zr dimer; there is one fully occupied  $d\pi$  orbital and one unoccupied  $d\pi$  orbital on each metal center. Differences in M  $\rightarrow$  N  $1\pi_g$  donation are observed because each of the Nb  $d\pi$  MOs are closer to the  $N_2$   $1\pi_g$  in electron volts than the Zr  $d\pi$  MOs and because the electrons in the lower energy Zr  $d\pi$  MO are tied up in back-bonding to the terminal  $N_2$  ligand. Mulliken populations show that 0.93 electron has been donated out of each Nb fragment 17a MO and that 0.23 electron has been accepted by MO 20a. In addition to increased M  $d\pi$  donation, synergetic  $\mu$ - $N_2$   $\sigma \rightarrow$  M donation is observed in the Nb case. Tables II and III show that more electrons have been donated out of the Nb dimer  $\mu$ - $N_2$  MO 3 $\sigma_g$  than out of the other  $\pi$ - $N_2$  3 $\sigma_g$  orbitals and that Nb fragment MOs 18a and 21a accept the donated electrons.

In their discussion of  $\{[Ta(CHCMe_3)(PMe_3)_2(CH_2CMe_3)]_2(N_2)\}$ ,<sup>38</sup> Churchill and co-workers cited the  $\mu$ - $N_2$   $\pi^*$ -metal "back-donation" as the cause of the rotated and locked geometry. They suggested that these interactions raise the Ta-N bond order. Our calculations indicate that  $d\pi$  interactions and synergetic  $\sigma$  donation both contribute to stronger Ta-N bonds.

The long N-N bond in  $\{[TaCl_3(P(bz)_3)(THF)]_2(N_2)\}$ <sup>3b</sup> occurs with the identical halves of the molecule rotated and locked at 180°, rather than 90°. If the metal fragments making our model dimer,  $\{[Nb(CH_2)(CH_3)(PH_3)_2]_2(N_2)\}$ , are rotated so that the  $PH_3$  groups are eclipsed and the molecule contains a center of inversion, the MO pattern is altered. The most significant change is that the 2e MO is split. The two filled Nb  $d\pi$  orbitals are oriented in the same plane, which also contains the alkyl and alkylidene ligands. These orbitals interact with the  $N_2$   $1\pi_g$  orbital to form a MO that is 25%  $N_2$   $1\pi_g$  and 75% Nb  $d\pi$  in character. The  $N_2$   $1\pi_g$  MO in this plane has an occupation of 0.61 electron. In the perpendicular plane, the two unoccupied Nb  $d\pi$  orbitals interact more strongly with the  $N_2$   $1\pi_g$  orbitals to form a MO that is 51%  $N_2$   $1\pi_g$  in character and 49% Nb  $d\pi$  in character. As a result of the strong  $N_2$   $1\pi_g$  participation, more electrons are donated into the  $N_2$   $1\pi_g$  MO in this plane; the electron population is 1.07.

The average  $1\pi_g$  population for the Nb dimer locked at 180° is 0.84 electron, which is  $\sim$ 0.08 electron higher than the  $1\pi_g$  occupation for the same molecule locked at 90°. Our calculations suggest that a Ta dimer locked in this geometry with ligands similar to those in the model would have the longest N-N bond length yet observed. It would be interesting to see if bidentate phosphines could be used to "tie" a molecule in this geometry.

**Conclusions.** In summary, our calculations suggest that the 3e MOs for all of the  $\mu$ - $N_2$  dimers are either nonbonding or very weakly bonding in character so that their occupation

(24) Calculations on the Nb and Zr dimers at the correct M-N bond distances, but the same N-N bond distances, give lower  $\mu$ - $N_2$   $1\pi_g$  populations for the Zr molecule and higher  $\mu$ - $N_2$   $1\pi_g$  populations for the Nb molecule, as expected.

cannot effect the N-N bond length. Thus, the character of the 2e MO must control the strength of the M-N and N-N bonds. The Ru dimer has the shortest N-N bond length due to less  $M \rightarrow N_2 1\pi_g$  donation, which results from less  $N_2$  participation in the 2e MO. More electrons are donated into the  $\mu-N_2 \pi^*$  system in the mixed-metal Re-Mo dimer, the Nb dimer, and the Zr dimer because the two unoccupied  $d\pi$  orbitals located at higher energy than the two occupied  $d\pi$  orbitals stabilize the  $\mu-N_2 1\pi_g$  MO. This allows the  $1\pi_g$  MO to participate more strongly in the 2e MOs. In the Re-Mo case both high-energy  $d\pi$  orbitals are primarily Mo  $d\pi$  in character. The Nb and Zr dimers have one occupied and one unoccupied  $d\pi$  orbital localized on each metal center. As a

result,  $M \rightarrow N_2 1\pi_g \rightarrow M$  electron flow can occur without charge depletion or charge buildup. Synergetic  $\sigma$  donation is observed for the Nb dimer, which strengthens the M-N bond and weakens the N-N bond.

The key to ambient-temperature nitrogen fixation may lie in  $d^2$  systems like those of Zr and Ta, where the N-N bond is lengthened by  $\pi$ -type synergism.

**Acknowledgment.** We thank the National Science Foundation (Grant No. CHE 83-09936 and CHE 79-20993) for their support.

**Registry No.**  $[\{Ru(NH_3)_5(N_2)\}^{4+}]$ , 25754-89-6;  $[\{Nb(PH_3)_2(C_6H_5)(CH_3)_2(N_2)\}]$ , 93383-47-2;  $[\{Zr(C_6H_5)_2(N_2)_2\}]$ , 93383-48-3;  $[\{Re(PH_3)_4Cl\}\{MoCl_4(OH)\}(N_2)]$ , 93383-49-4.

Contribution from the Department of Chemistry,  
Texas A&M University, College Station, Texas 77843

## Generalized Molecular Orbital Calculations on Transition-Metal Dioxygen Complexes. Models for Iron and Cobalt Porphyrins

JAMES E. NEWTON and MICHAEL B. HALL\*

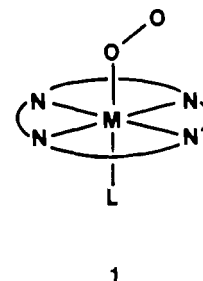
Received April 11, 1984

Generalized molecular orbital calculations with configuration interaction are reported for the dioxygen complexes of Co and Fe. The other ligands include a model ligand to represent the porphyrin ring system and a trans ammonia. The Co-O<sub>2</sub> system is best described as a superoxide complex,  $Co^{3+}-O_2^-$ , with the unpaired electron in a nearly pure  $\pi_g O_2$  orbital. The Fe-O<sub>2</sub> system is best described as a singlet dioxygen,  $O_2 (^1\Delta_g)$   $\sigma$  donating to and  $\pi$  accepting from an  $Fe^{2+}$ . All of the experimental results for both systems can be rationalized with these descriptions. The calculations predict a low-lying triplet state for the FeO<sub>2</sub> system, but not low enough in energy to explain the recently reported paramagnetism of hemoglobin.

### Introduction

Transition-metal dioxygen complexes continue to generate considerable interest.<sup>1</sup> Although relatively few of these complexes are biologically active, studies on model systems of both iron and cobalt have increased our understanding of the chemistry and structure of the biological systems. Evidence accumulated from X-ray studies on iron<sup>2</sup> and cobalt<sup>3</sup> model compounds and structural work on oxymyoglobin<sup>4</sup> lead to the conclusion that in these and oxyhemoglobin the metal is six-coordinate with an end-on, bent MO<sub>2</sub> linkage, **1**, where it can be accurately determined the O-O distance in iron porphyrins is 1.23-1.25 Å, while in cobalt complexes it is 1.26-1.30 Å. The metal to oxygen distances are substantially different; Fe-O distances are 1.70-1.75 Å while Co-O distances are 1.86-1.89 Å. The M-O-O angles are larger for Fe(135-130°) than for Co (120-115°).

The vast amount of experimental work on both metals, which will not be reviewed here, can be accommodated with either a  $M^{2+}-O_2^0$  (dioxygen) or a  $M^{3+}-O_2^-$  (superoxide) de-



scription. Recent theoretical work has included extended Pariser-Parr-Pople and  $X\alpha$  multiple scattering calculations,<sup>5</sup> which suggest that the FeO<sub>2</sub> unit could be viewed as an equal mixture of  $Fe^{2+} (S = 0)-O_2^0 (S = 0)$  and  $Fe^{2+} (S = 1)-O_2^0 (S = 1)$ . The latter description, which resembles ozone, was suggested as the major contributor by generalized valence bond calculations.<sup>6</sup> However, other ab initio calculations suggest that  $Fe^{2+} (S = 0)-O_2^0 (S = 0)$  plays the dominant role in the ground state.<sup>7</sup> Further confusion is added by recent INDO-SCF-CI calculations which suggest that the ground state has considerable  $Fe^{3+} (S = 1/2)-O_2^- (S = 1/2)$  character.<sup>8</sup> Pauling

- Gubelmann, M. H.; Williams, A. F. *Struct. Bonding (Berlin)* **1983**, 55, 1. Boca, R. *Coord. Chem. Rev.* **1983**, 50, 1. Smith, T. D.; Pilbrow, J. R. *Coord. Chem. Rev.* **1981**, 39, 395. Vaska, L. *Acc. Chem. Res.* **1976**, 9, 175. Basolo, F.; Hoffman, B. M.; Ibers, J. A. *Acc. Chem. Res.* **1975**, 8, 384. Summerville, D. A.; Hoffman, B. M.; Basolo, F. *J. Chem. Educ.* **1981**, 14, 102. McLendon, G.; Martell, A. E. *Coord. Chem. Rev.* **1976**, 19, 1. Wilkins, R. *Adv. Chem. Ser.* **1971**, No. 100, 111. Paris, M. R.; Aymes, D. *Bull. Soc. Chim. Fr.* **1976**, 1, 431.
- Collman, J. P.; Gagné, R. R.; Reed, C. A.; Robinson, W. T.; Rodley, G. A. *Proc. Natl. Acad. Sci. U.S.A.* **1974**, 71, 1326. Collman, J. P.; Gagné, R. R.; Reed, C. A.; Halbert, T. R.; Lang, G.; Robinson, W. T. *J. Am. Chem. Soc.* **1975**, 97, 1427. Jameson, G. B.; Rodley, R. R.; Reed, C. A.; Collman, J. P. *Inorg. Chem.* **1978**, 17, 850. Collman, J. P.; Suslick, K. S. *Pure Appl. Chem.* **1978**, 50, 951. Jameson, G. B.; Molinaro, F. S.; Ibers, J. A.; Collman, J. P.; Brauman, J. I.; Rose, E.; Suslick, K. S. *J. Am. Chem. Soc.* **1980**, 102, 3224.
- Gall, R. S.; Schaefer, W. P. *Inorg. Chem.* **1976**, 15, 2. Gall, R. S.; Rogers, J. F.; Schaefer, W. P.; Christoph, G. C. *J. Am. Chem. Soc.* **1976**, 98, 5135. Hine, B. T.; Heyden, R. M.; Schaefer, W. P. *Inorg. Chem.* **1979**, 18, 125. Avdeff, A.; Schaefer, W. P. *J. Am. Chem. Soc.* **1976**, 98, 5153.
- Phillips, S. E. V. *Nature (London)* **1978**, 273, 247; *J. Mol. Biol.* **1980**, 142, 531.

- Huynh, B. H.; Case, D. A.; Karplus, M. *J. Am. Chem. Soc.* **1977**, 99, 1603. Case, D. A.; Huynh, B. H.; Karplus, M. *J. Am. Chem. Soc.* **1979**, 101, 4433.
- Goddard, W. A., III; Olafson, B. D. *Proc. Natl. Acad. Sci. U.S.A.* **1975**, 72, 2335. Olafson, B. D.; Goddard, W. A., III. *Proc. Natl. Acad. Sci. U.S.A.* **1977**, 74, 1315.
- Dedieu, A.; Rohmer, M.-M.; Veillard, A. *Adv. Quantum Chem.* **1982**, 16, 43. Dedieu, A.; Rohmer, M.-M.; Benard, M.; Veillard, A. *J. Am. Chem. Soc.* **1976**, 98, 3713. Dedieu, A.; Rohmer, M.-M.; Veillard, H.; Veillard, A. "Metal-Ligand Interactions in Organic Chemistry and Biochemistry"; Pullman, B., Goldblum, N., Eds.; D. Reidel: Dordrecht, Holland, 1977; Part 2, p 101. Veillard, A.; Dedieu, A.; Rohmer, M.-M. "Horizons of Quantum Chemistry"; Fukui, F., Pullman, B., Eds.; D. Reidel: Dordrecht, Holland, 1980; p 197.
- Herman, Z. S.; Loew, G. H. *J. Am. Chem. Soc.* **1980**, 102, 1815. Kirchner, F. R.; Loew, G. H. *J. Am. Chem. Soc.* **1977**, 99, 4639. Loew, G. H.; Kirchner, R. F. *Int. J. Quantum Chem., Quantum Biol. Symp.* **1978**, No. 5, 403. Loew, G. H.; Herman, Z. S.; Zerner, M. C. *Int. J. Quantum Chem.* **1980**, 18, 481.